The Astrophysical Journal, 681:1089–1098, 2008 July 10

TOWARD A ROBUST ESTIMATE OF THE MERGER RATE EVOLUTION USING NEAR-IR PHOTOMETRY

A. Rawat,[1,2] Francois Hammer,[2] Ajit K. Kembhavi,[1] and Hector Flores[2]

Received 2007 June 19; accepted 2008 March 31

ABSTRACT

We use a combination of deep, high angular resolution imaging data from the CDFS (*HST*/ACS GOODS survey) and ground-based near-IR K_s images to derive the evolution of the galaxy major merger rate in the redshift range $0.2 \leq z \leq 1.2$. We select galaxies solely on the basis of their *J*-band rest-frame absolute magnitude, which is a good tracer of the stellar mass. We find steep evolution with redshift, with the merger rate $\propto(1+z)^{3.43\pm0.49}$ for optically selected pairs and $\propto(1+z)^{2.18\pm0.18}$ for pairs selected in the near-IR. Our result is unlikely to be affected by luminosity evolution that is relatively modest when using rest-frame *J*-band selection. The apparently more rapid evolution that we find in the visible is likely caused by biases relating to incompleteness and spatial resolution affecting the ground-based near-IR photometry, underestimating pair counts at higher redshifts in the near-IR. The major merger rate was ~5.6 times higher at $z \sim 1.2$ than at the current epoch. Overall, $41\% \times (0.5\ \mathrm{Gyr}/\tau)$ of all galaxies with $M_J \leq -19.5$ have undergone a major merger in the last ~8 Gyr, where τ is the merger timescale. Interestingly, we find no effect on the derived major merger rate due to the presence of the large-scale structure at $z = 0.735$ in the CDFS.

Subject headings: galaxies: evolution — galaxies: formation — galaxies: interactions — galaxies: statistics

1. INTRODUCTION

Galaxy mergers are believed to be the chief mechanism driving galaxy evolution within the hierarchical framework. Although mergers are rare at the current epoch, the hierarchical framework predicts that the merger rate must have been higher at earlier epochs. Despite its importance in understanding galaxy evolution, the quantification of the galaxy major merger rate and its evolution with redshift is still an ill-constrained and hotly debated issue. Patton et al. (1997) have derived a clear increase in the merger fraction with redshift until $z \sim 0.33$ with a power-law index of 2.8 ± 0.9. However, extension of this work to higher redshifts has been riddled with controversy. Le Fevre et al. (2000) reported steep evolution of the major merger rate until $z \sim 1.0$, with a power-law index of 3.2 ± 0.6 using pair-counting in the optical band for identifying the merger candidates. Bundy et al. (2004) reported a much more modest evolution of merger rate using K'-band images for identifying major merger candidates. Lin et al. (2004) also reported very weak evolution in the merger rates using the DEEP2 redshift survey. Bell et al. (2006) reported a fairly rapid evolution in merger fraction of massive galaxies between $z \sim 0.8$ and the current epoch, using the technique of projected two-point correlation function. Lotz et al. (2008), on the other hand, reported that the major merger fraction remains roughly constant at ~10% ± 2% until $z \sim 1.2$, using a nonparametric technique for quantifying galaxy morphology. Some of the discrepancies in the results quoted above may be attributed to differences in sample selection criteria, different techniques to derive the merger rate, and different definitions of major mergers used by various people.

We have used a combination of high-resolution imaging data from the *HST*/ACS GOODS survey and K_s imaging data from the VLT follow-up of the GOODS-South field to quantify the major merger rate of galaxies and its redshift evolution using the technique of pair counting. Section 2 lists the data sets we have used in this work and briefly explains the methodology that we have employed in this paper for deriving the merger rate. Section 3 details the sample selection criterion employed by us and the possible biases in our sample. Section 4 explains the details of the photometry performed by us in the K_s filter. Section 5 explains in detail how we identify major pairs of galaxies, along with correcting for possible contamination and incompleteness issues. Section 6 compares the differences in pairs identified in the visible and the near-IR. Section 7 deals with the calculation of the major merger rate from our identified pairs and its evolution with redshift. We conclude by discussing the implications of our results obtained in this paper in Section 8. We adopt a cosmology with $H_0 = 70$ km s^{-1} Mpc^{-1}, $\Omega_M = 0.3$, and $\Omega_\Lambda = 0.7$.

2. THE DATA

We have used version v1.0 of the reduced, calibrated images of the *Chandra* Deep Field–South (CDFS) acquired with *HST*/ACS as part of the GOODS survey (Giavalisco et al. 2004). The SExtractor (Bertin & Arnouts 1996) based version r1.1 of the ACS multiband source catalogs was used for object identification. Spectroscopic redshifts were taken from the redshift catalog of the VVDS (Le Fevre et al. 2004), GOODS/FORS2 redshift survey (Vanzella et al. 2005, 2006), and the IMAGES survey (Ravikumar et al. 2007). The near-IR *J*- and K_s-band imaging data of the GOODS/CDFS region from the ESO GOODS/EIS Release version 1.5 (B. Vandame et al. 2008, in preparation) was used.

2.1. *The Methodology*

The methodology that we employ in this paper is quite straightforward. First, we identify sources with known spectroscopic redshifts in the GOODS-S field. We then shortlist those galaxies with redshift in the range $0.2 \leq z \leq 1.2$ and rest-frame absolute magnitude brighter than $M_J(\mathrm{AB}) = -19.5$ to obtain a volume-limited sample of primary galaxies. We then identify neighbors within a projected radius of $5\ h_{100}^{-1}$ kpc $\leq r \leq 20\ h_{100}^{-1}$ kpc around each

[1] Inter-University Centre for Astronomy and Astrophysics, Post Bag 4, Ganeshkhind, Pune 411007, India; rawat@iucaa.ernet.in.
[2] GEPI, L'Observatoire de Paris-Meudon, 92195 Meudon, France.

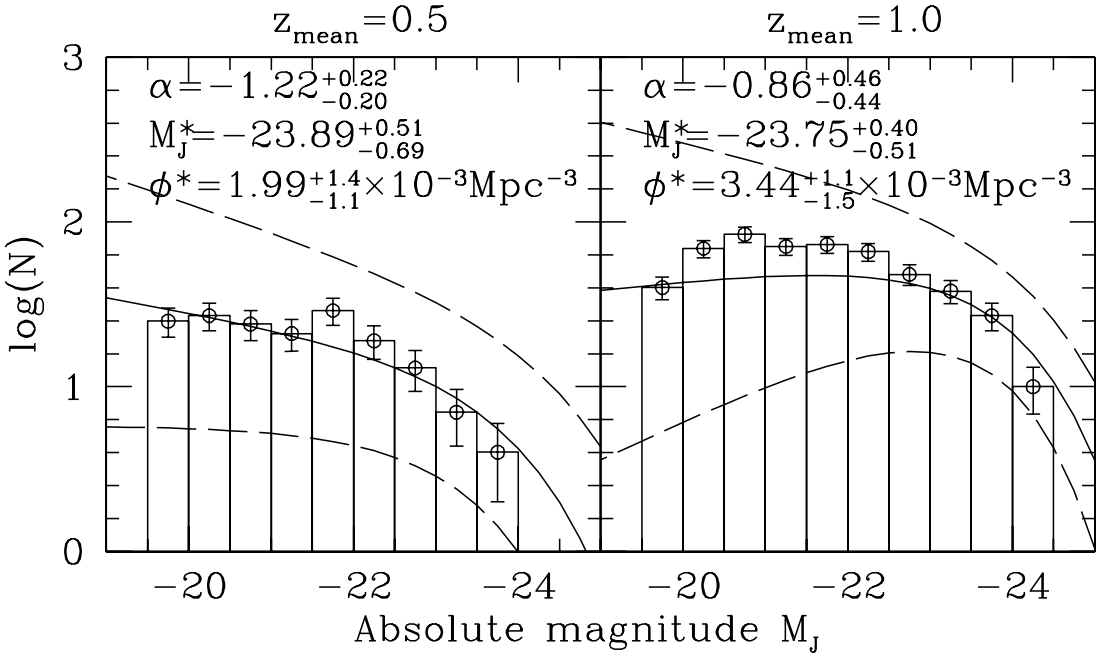

FIG. 1.—Comparison between the luminosity distribution of our sample galaxies in the redshift range $0.2 \leq z \leq 0.65$ (*left*) and $0.65 \leq z \leq 1.2$ (*right*), respectively, and the distribution predicted by the luminosity function of Pozzetti et al. (2003). The solid line is the luminosity distribution predicted by the mean values of α, M^*, and ϕ^* given by Pozzetti et al. (2003), whereas the two dashed lines on either side demarcate the 1 σ region around the mean as parameterized by the error bars on α, M^*, and ϕ^* mentioned above.

primary galaxy. If the difference in the apparent magnitude δm of the primary galaxy and the neighbor satisfy the condition $-1.5 \leq \delta m \leq 1.5$ in either the z or K_s filters, the galaxy pair is designated to be a *major pair* in that particular filter. This is explained in § 5.

We do not have the redshift for the secondary member of a major pair in most cases, and as such some of them can simply be foreground/background superpositions. Such a contamination is statistically corrected by using number counts of objects in the field in the z or K_s filters and is explained in detail in § 5.1. Our primary galaxy sample is then binned into three redshift bins. The fraction of galaxies undergoing major merger in any given redshift bin is then inferred from the fraction of galaxies existing in major pairs in the same bin, after applying a correction for foreground/background contamination. The evolution in the major merger fraction is then determined by looking for any change in the major merger fraction over the three redshift bins that we have.

3. SAMPLE SELECTION AND POSSIBLE BIASES

We cross-correlated the *HST*/ACS source catalog with the three redshift catalogs mentioned above to yield objects with spectroscopic redshifts in the range $0.2 \leq z \leq 1.2$. Since we have used spectroscopic redshifts from various surveys in the CDFS for the sample selection, our sample is liable to suffer from the same biases as those induced at the time of target selection by the spectroscopic surveys. The IMAGES survey is biased toward brighter galaxies with strong emission lines (Ravikumar et al. 2007). The shorter integration times used in the IMAGES survey result in poor signal-to-noise ratio for fainter galaxies and results in difficulties in estimating redshifts for galaxies that exhibit only absorption lines or weak emission lines. Hence, they are biased against faint, red early-type galaxies. However, this bias is recovered to a large extent by the sample selection criterion of the GOODS/FORS2 redshift survey (Vanzella et al. 2005), which is tailor-made to exploit the red throughput and sensitivity of FORS2. This preferentially selects red, faint early-type galaxies and provides a nice complementary redshift catalog to the IMAGES survey. Indeed, this has been discussed at length by Ravikumar et al. (2007; see their § 4.1), who have successfully tested the representativeness of the combination of IMAGES and FORS2 sample. The VVDS survey, on the other hand, is quite unbiased owing to the simple selection criterion of apparent magnitude $I_{AB} \leq 24.0$ and does not bias for or against any particular type of object (Le Fevre et al. 2004). The recovery success rate for the three redshift surveys vary from 88% for the VVDS, 77% for GOODS/FORS2, and 76% for the IMAGES survey. In addition to this, the above mentioned recovery rates are a function of magnitude of the object (see Le Fevre et al. 2004; Vanzella et al. 2005; Ravikumar et al. 2007). Therefore, as in any flux-limited survey, fainter objects with weaker or no emission lines (e.g., red absorption line galaxies) are underrepresented. This caveat must be kept in mind while interpreting the results presented in this paper. In spite of the limitations imposed by the flux-limited nature of the surveys, a combination of these three redshift catalogs yields a sample of galaxies that is reasonably representative of the field galaxy population out to a redshift of $\sim$1.2.

Galaxies with rest-frame absolute magnitude brighter than $M_J(\mathrm{AB}) = -19.5$ have been selected as the primary galaxies, leaving us with 695 galaxies. The luminosity cutoff was selected to ensure that the sample does not suffer from any incompleteness (Malmquist bias) in the highest redshift bin. The rest-frame J band is significantly less affected by sporadic star formation than bluer bands and is more representative of the stellar mass content. Figure 1 illustrates that the resulting sample is rather well representative of the Schechter luminosity function from Pozzetti et al. (2003) at mean redshift $z_{\mathrm{mean}} \sim 0.5$ and 1.0. The Schechter luminosity function is parameterized as

$$\phi(M) = 0.9210\phi^* 10^{0.4(\alpha+1)(M^*-M)} \times e^{-10^{0.4(M^*-M)}}, \quad (1)$$

where the values of α, M^*, and ϕ^* from Pozzetti et al. (2003) are given in Figure 1.

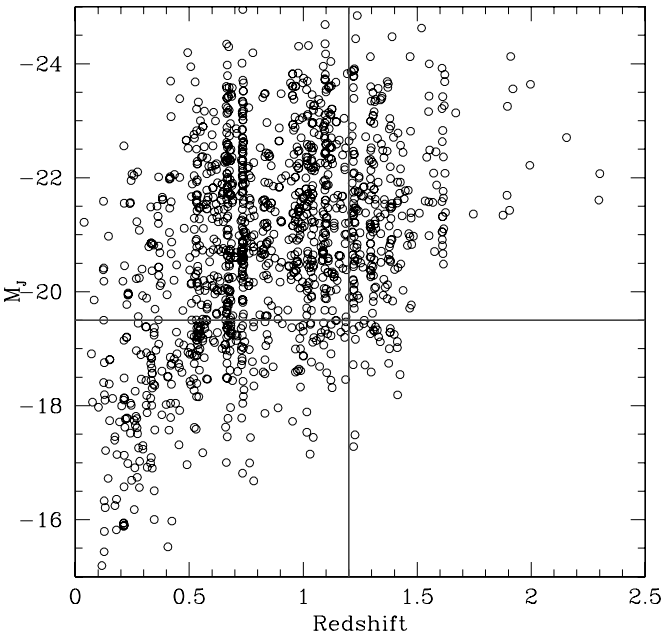

FIG. 2.—Pictorial representation of the sample selection criterion applied by us in terms of redshift and luminosity cutoffs. Note the prominent large-scale structure at $z \sim 0.735$.

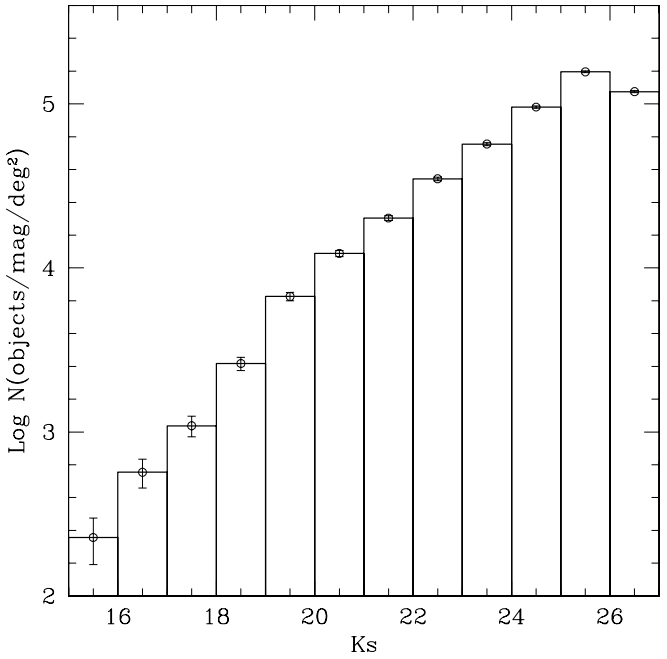

FIG. 3.—K_s-band differential number counts obtained using the SExtractor catalog that we have constructed.

Figure 2 shows pictorially the sample selection criterion applied by us in terms of redshift and luminosity cutoffs.

4. K_s-BAND PHOTOMETRY

Near-infrared imaging observations of the CDFS have been carried out, as part of GOODS, in J, H, and K_s bands using VLT/ISAAC. In the present work, we have used the ESO GOODS/EIS Release version 1.5 (B. Vandame et al. 2008, in preparation). This data release includes 24 fully reduced VLT/ISAAC fields in J and K_s bands, covering 159.1 and 159.7 arcmin^2 of the GOODS/CDFS region, respectively.

We have carried out photometry with SExtractor on the J and K_s images, using DETECT_THRESH=1.0, DETECT_MINAREA=5, and DEBLEND_MINCONT=0.0005 in both filters. Deblending is a major source of worry when studying close pairs of objects. However, we are essentially immune to this problem as our selection criteria demand that the fainter member of a pair have at least 25% of the flux of the other member to qualify as a major pair. Hence, even if SExtractor ends up splitting a source into two (or more) owing to a low value of DEBLEND_MINCONT, it will still not get counted as a legitimate major pair. The combination of DETECT_THRESH, DETECT_MINAREA, and DEBLEND_MINCONT has been optimized after several iterations of experimenting with different values for these parameters and subsequent visual examination after overlaying the derived catalog onto the J- and K_s-band images. The differential number counts obtained using our SExtractor catalog are given in Figure 3.

5. FINDING PAIRS OF GALAXIES

We have used a simple prescription for finding pairs of galaxies by identifying neighbors within a projected radius of 20 h_{100}^{-1} kpc for each of the 695 main galaxies. For each neighbor, we find the difference in the magnitude δm of the main galaxy and the neighbor in the z as well as K_s filters separately. If the condition $-1.5 \leq \delta m \leq 1.5$ is satisfied in at least one of the two filters, the pair is designated to be a tentative *major pair* in that particular filter. This condition ensures that the fainter member of the pair has at least 25% of the z- or K_s-band flux of the brighter member. It is important to note here that it is entirely possible for a neighbor to be *brighter* than the primary galaxy. It may indeed happen that a fainter galaxy within a pair has a spectroscopic measurement, while the brighter galaxy has none, owing to observing constraints of the redshift survey.

Not including brighter neighbors can lead to an underestimation of the derived merger fraction. We find that by not including major pairs in which the neighbor is brighter than the primary galaxy, we underestimate the number of major pairs by 34% in the K_s filter and 24% in the z filter. The importance of including brighter companions in the definition of major pairs has been missed by earlier workers in the field.

The simple selection criterion employed by us yielded a sample of 162 and 226 tentative major pair candidates in the K_s and z filters, respectively. We do not have the redshift for the secondary member of a pair in most cases; therefore, some of them can simply be foreground/background superpositions. Such a contamination can be statistically corrected for by using number counts of objects in the field and is explained in § 5.1. However, in the cases in which the secondary member does have a redshift, we have used it to rule out those apparent pairs from the list that are obviously at different redshift compared to the host galaxy. This left us with 125 and 181 major pair candidates in the K_s and z filters, respectively. Furthermore, a lower limit of 5 h_{100}^{-1} kpc is imposed on the separation between the major pair candidates and the main galaxy in order to avoid confusing clumpy extensions of the main galaxy itself as a neighbor. This left us with 119 and 170 major pair candidates in the K_s and z filters, respectively. These major pair candidates are then segregated into three redshift bins and are listed in Table 1. Figure 4 shows a montage of z-band *HST*/ACS images of some of the confirmed major pairs, identified in the z filter, where the secondary member has the same spectroscopic redshift as the host galaxy. Similarly, Figure 5 shows K_s-band images of some of the confirmed major pairs identified in the K_s filter. Note that there is a one-to-one correspondence between the first four objects in Figures 4 and 5.

TABLE 1
PAIR STATISTICS

z	$N_{\rm host}$	$N_{\rm pairs}^{\rm F850LP}$	$N_{\rm pairs}^{\rm F850LP}$(conf.)	$N_{\rm proj.}^{\rm F850LP}$	$N_{\rm pairs}^{K_s}$	$N_{\rm pairs}^{K_s}$(conf.)	$N_{\rm proj.}^{K_s}$	$f(z)$(F850LP)	$f(z)(K_s)$
0.20–0.50.....	61	4	0	0.70	5	0	0.81	2.70 ± 1.67	3.43 ± 1.87
0.50–0.75.....	294	48	7	19.56	39	3	9.76	6.03 ± 1.30	5.48 ± 1.14
0.75–1.20.....	340	98	13	42.94	62	10	18.80	10.01 ± 1.64	7.82 ± 1.31
Total	695	150	20	63.20	106	13	29.37	...	...

NOTES.—$N_{\rm host}$ is the number of primary galaxies in each redshift bin. $N_{\rm pairs}$ is the number of galaxies existing in major pairs within *projected* 5 h_{100}^{-1} kpc $\leq r \leq$ 20 h_{100}^{-1} kpc of the primary galaxies in each of the two filters. $N_{\rm pairs}$(conf.) is the number of galaxies spectroscopically confirmed to be existing in *major* pairs. $N_{\rm proj.}$ is the number of major neighbors expected to be found within 5 h_{100}^{-1} kpc $\leq r \leq$ 20 h_{100}^{-1} kpc of the primary galaxies by pure chance coincidence, estimated statistically using number counts of sources in each of the two filters. Merger fraction is estimated as $[N_{\rm pairs} + N_{\rm pairs}({\rm conf.}) - N_{\rm proj.}]/N_{\rm host} \times 0.5$. The error bars are estimated using Poisson statistics.

We have used the z as well as the K_s filters to define major mergers because the former filter allows us to find companions very near to the primary galaxy (thanks to the exquisite spatial resolution of the ACS camera) and the latter is less affected by star formation and more representative of the stellar mass (e.g., Bundy et al. 2004).

5.1. *Estimation of the Foreground/Background Contamination*

Since we do not have redshift for the secondary member of a pair in most cases, some of them can simply be foreground/background superpositions. Such a contamination can be statistically corrected by using number counts of objects in the field in

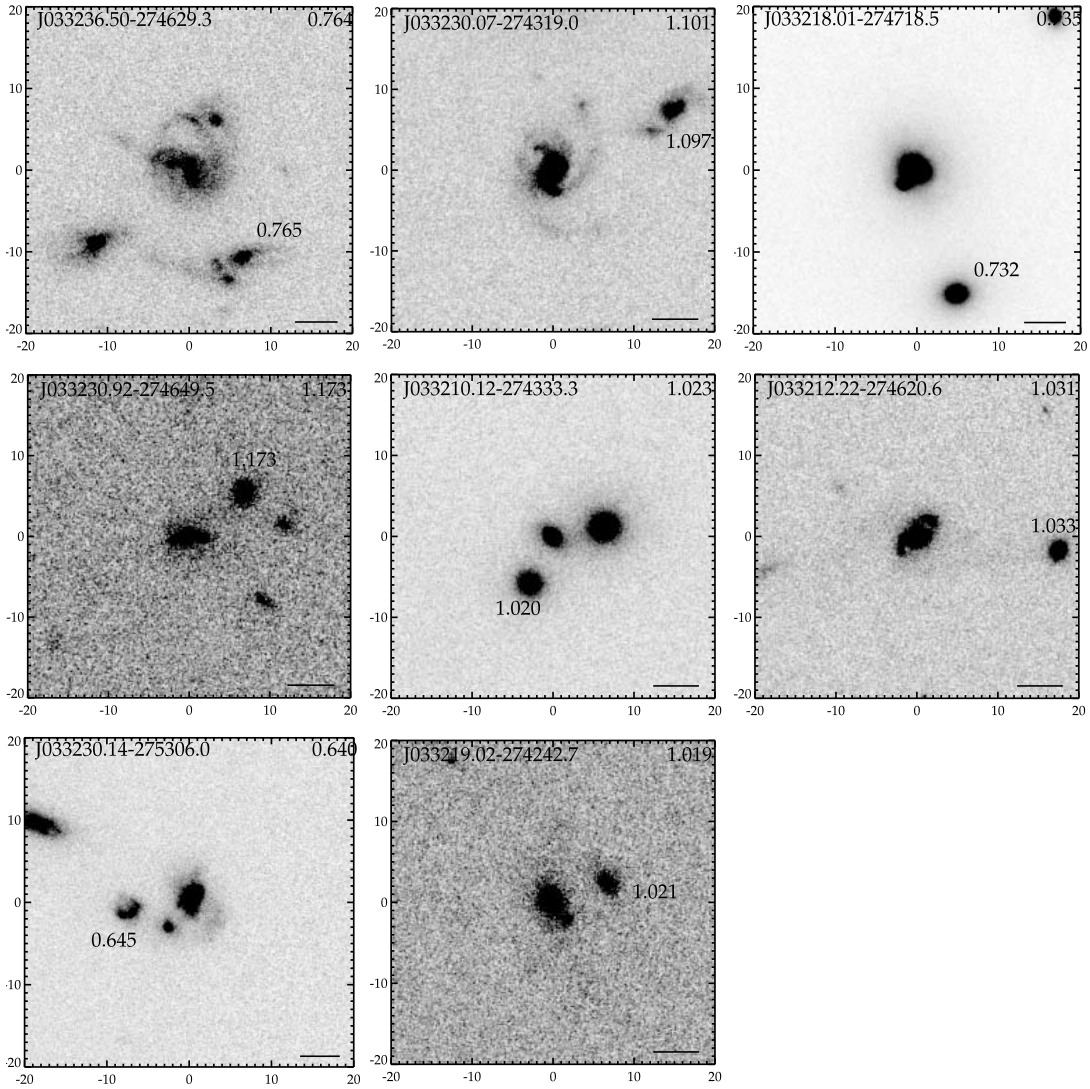

FIG. 4.—Montage of z-band *HST*/ACS images of some of the confirmed major pairs, identified in the z filter, where the secondary member has the same spectroscopic redshift as the host galaxy. Each image is 40 × 40 h_{100}^{-1} kpc in size. The unique object ID of the host galaxy is marked on the top left of each image, the redshift of the host galaxy is marked on the top right, and the redshift of the neighbor is marked next to it. The horizontal bar on the bottom right shows a scale of 1″.

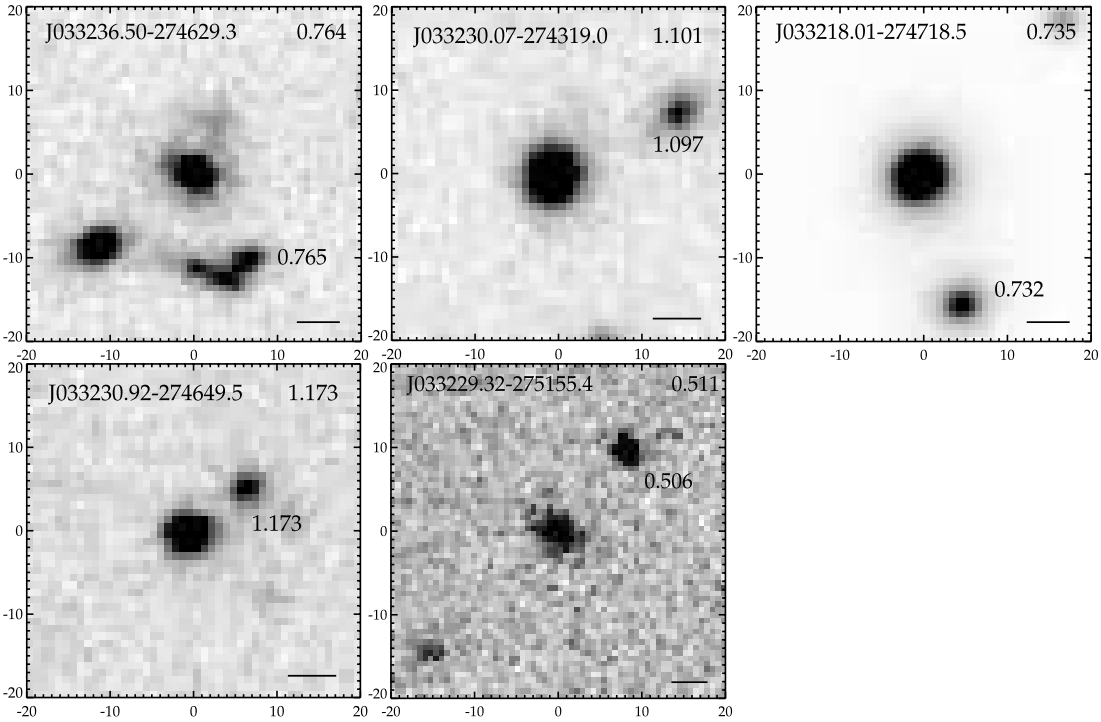

FIG. 5.—Montage of K_s-band images of some of the confirmed major pairs, identified in the K_s filter, where the secondary member has the same spectroscopic redshift as the host galaxy. Each image is 40×40 h_{100}^{-1} kpc in size. The unique object ID of the host galaxy is marked on the top left of each image, the redshift of the host galaxy is marked on the top right, and the redshift of the neighbor is marked next to it. The horizontal bar on the bottom right shows a scale of 1″.

the z or K_s filters to estimate the probability of finding an object within projected 5 h_{100}^{-1} kpc $\leq r \leq$ 20 h_{100}^{-1} kpc of the main galaxy and within ± 1.5 mag of the main galaxy. This statistically expected number can then be subtracted off the number of neighbors observed around a given host galaxy to yield the number of true neighbors for that particular host. Mathematically, this statistical correction is calculated as

$$\int_{m-1.5}^{m+1.5} N(m')\, dm' \pi \left(r^2_{20\, h_{100}^{-1}\ \mathrm{kpc}} - r^2_{5\, h_{100}^{-1}\ \mathrm{kpc}} \right), \qquad (2)$$

where $N(m')$ is the differential number counts of objects in a given filter, m is the apparent magnitude of the host galaxy in the same filter, and $r_{20\, h_{100}^{-1}\ \mathrm{kpc}}$ and $r_{5\, h_{100}^{-1}\ \mathrm{kpc}}$ are the projected radius in degrees corresponding to 20 and 5 h_{100}^{-1} kpc at the redshift of the main galaxy. In the K_s band, these number counts were established by using the SExtractor catalog as explained in § 4. In the z band, we have estimated the number counts using the catalog published by the GOODS team.

Equation (2) gives us the number of sources that are expected to be present within ± 1.5 mag and within projected 5 h_{100}^{-1} kpc $\leq r \leq$ 20 h_{100}^{-1}kpc of the host galaxy by pure chance coincidence. It may be noted that this statistical correction is only calculated (and subtracted) in those cases in which the neighbor does not have a spectroscopic redshift. If the neighbor has a spectroscopic redshift, then we know for sure whether or not it is a real pair; hence, there is no need to apply the statistical correction.

This number is calculated for every host galaxy in our sample that has a neighbor without a redshift. The final number is listed in Table 1, segregated into three redshift bins, summed over all the host galaxies (with neighbors sans redshift) in a given redshift bin.

5.2. *Test of Our Contamination Calculation*

We tested the accuracy of our statistically estimated foreground/background contamination derived in § 5.1 in two ways. First, we compute the ratio of the statistically expected neighbors to the number of major neighbors actually found in projection as listed in Table 1. This can be termed as a sort of "contamination rate." This contamination rate is then compared to earlier works of Le Fevre et al. (2000). The contamination rate that we find here (in the z band) is $42\% \pm 6.3\%$. This is in excellent agreement with the contamination rate of $49\% \pm 13\%$ (as derived from Table 3 of Le Fevre et al. 2000). This agreement gives us additional confidence in our estimate of the foreground/background contamination.

In addition to our comparison with earlier works, we also checked our contamination rate of $42\% \pm 6.3\%$ with the contamination rate derived using the subset of our major pairs where we have spectroscopic redshifts for both members of the pair. There are 65 major pairs in the z band where both members of the pair have spectroscopic redshifts. In order to establish how many of these 65 major pairs are indeed at the *same* redshift, we plotted a histogram of $\delta z/(1+z) = (z_{\mathrm{host}} - z_{\mathrm{neigh}})/(1+z_{\mathrm{host}})$ for these 65 major pairs. This is shown in Figure 6. It turns out that there are a number of pairs with $-0.006 \leq \delta z/(1+z) \leq 0.006$, which are presumably located at the *same* redshift, with the residual difference in redshift $\delta z/(1+z)$ being attributed to redshift measurement errors and peculiar velocities of the members.

A $\delta z/(1+z) = 0.006$ corresponds to delta velocity of 1800 km s^{-1}. We were forced to use this seemingly large value of $\delta z/(1+z)$ due to the error bars on the spectroscopic redshifts of the objects. The quoted error bars in the redshift measurements are of the order $\sim$0.002 for VVDS and GOODS/FORS2 and $\sim$0.006 for the IMAGES survey. In addition to this, these quoted error bars are to be treated as lower limits due to the way in which they are calculated (see, e.g., Vanzella et al. 2005). Since we are using three different redshift surveys, we have taken to using the worst error bars, i.e., $\delta z/(1+z) = 0.006$. This implies that the delta velocity of 1800 km s^{-1} is to be treated as an upper limit, and the true delta velocity is liable to be smaller.

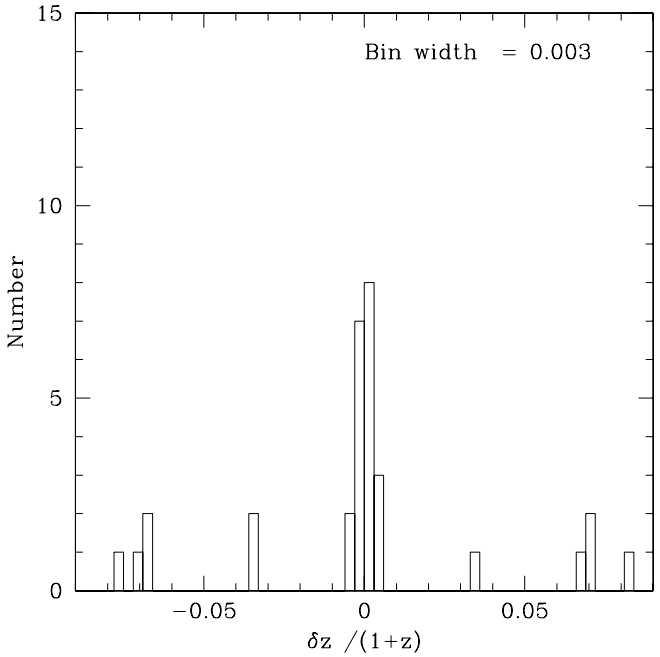

FIG. 6.—Histogram of $(z_{\rm host} - z_{\rm neigh})/(1 + z_{\rm host})$ for the 65 major pairs where both members have a spectroscopic redshift. Note that only 20 pairs have $-0.006 \leq \delta z/(1 + z) \leq 0.006$ as seen in the figure. Most other pairs have $\delta z/(1 + z)$ much larger than 0.006 so that they are out of the frame.

In Figure 6 many objects have $\delta z/(1 + z)$ much larger than 0.006 (so much so that most of them are out of the frame in Fig. 6). The members of such pairs are treated as having "discordant redshifts" and are essentially foreground/background superpositions. From this plot, we can then derive the fraction of pairs that are actually foreground/background superpositions (i.e., the contamination rate). This contamination rate is found to be $\sim$69% $\pm$ 13%. On first sight this might appear larger than the contamination rate of 42% $\pm$ 6.3% that we have obtained using our statistically estimated foreground/background contamination (although note the large error bars since we are dealing with small number statistics here). However, we checked the spectra of the pairs having discordant redshifts ourselves. It turns out that in many cases, the redshift determination can be quite poor indeed, especially in the low-exposure and low-resolution VVDS (as parameterized by their redshift flag). So in cases in which the neighbor has a VVDS redshift flag 2 (75% confidence) or worse, there is a much greater risk of the pair being designated as having discordant redshifts. In addition to this, one also has to allow for the fact that some of the pairs using redshifts from the other two redshift catalogs can also be erroneously counted as discordant (for the same reason as above). Such pairs account for $\sim$15/45 discordant redshift pairs in the z band. This can significantly swing the number of pairs with discordant redshifts. If we discard these 15 discordant cases and recalculate the contamination rate, we get 60% $\pm$ 14% as the contamination rate, which is in much better agreement with the contamination rate of 42% $\pm$ 6.3% that we have obtained using our statistically estimated foreground/background contamination.

In a nutshell, our contamination calculation is robust, and the contamination rate compares well with the contamination rate reported in literature, as well as with the subsample of our major pairs where we have spectroscopic redshifts for both members of the pair. Also, as a result of our eagerness to throw out prospective pairs as having discordant redshifts due to spurious redshift determination in some cases, we are going to end up with an estimate of merger fraction that is a bit too low, and thus it should be treated as a lower limit.

5.3. *Source Blending and Photometric Completeness*

A major bias when studying close pairs of objects may be caused by the fact that sources are blended when their separation is comparable to the PSF. It particularly affects ground-based K_s images because the K_s PSF ($\sim$0.5″) is much larger than the *HST* optical PSF ($\sim$0.1″). This is illustrated in Figure 7, where we have plotted the angular separation between the main galaxy and neighbors identified in the z filter against the z magnitude of the neighbor, segregated into three redshift bins. A neighbor here is identified as any galaxy within 5 h_{100}^{-1}kpc $\leq r \leq$ 20 h_{100}^{-1} kpc of the primary galaxy, regardless of its magnitude. The resultant list of 1085 neighbors includes major as well as minor neighbors and constitutes the pool from which the major pairs are identified. In Figure 7 the open circles denote neighbors that have K_s magnitudes, whereas the green crosses denote neighbors that do not have K_s magnitude. As is shown in Figure 7, there are a large number ($\sim$43%) of such neighbors that do not have K_s-band magnitudes. This has the consequence of reducing the pool of neighbors from which the major pairs are identified

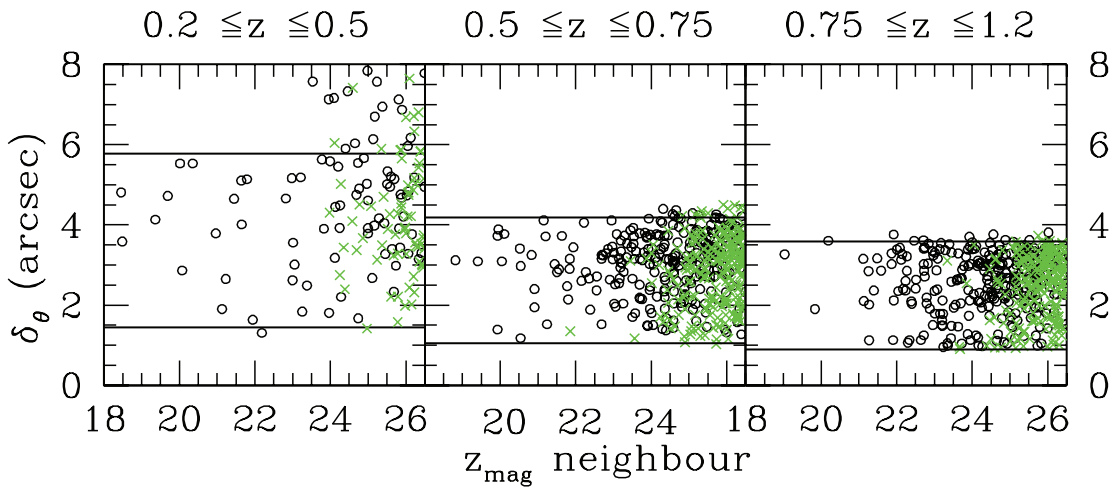

FIG. 7.—Angular separation between the main galaxy and the neighbor identified in the z filter vs. the z magnitude of the neighbor, segregated into three redshift bins as indicated. The open circles are neighbors that have measured K_s magnitude, whereas the green crosses are neighbors that do not have K_s magnitude. The horizontal lines correspond to 20 and 5 h_{100}^{-1} kpc at the mean redshift of each bin, respectively.

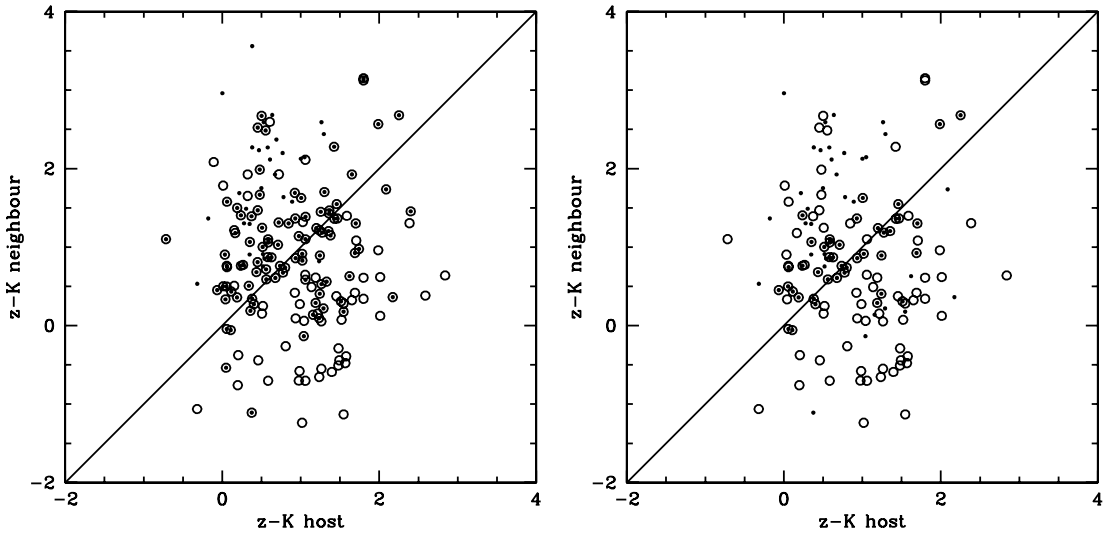

FIG. 8.—*Left*: $z - K_s$ color of the primary galaxy vs. that of the major neighbor ($-1.5 \leq \delta m \leq 1.5$) as described in § 6. The open circles and dots represent neighbors identified in the z and K_s filters, respectively. Not surprisingly, in the K_s filter we preferentially select neighbors that are redder than the primary galaxy, while a selection in the z filter selects bluer neighbors. *Right*: Similar to the left panel, except that only those major neighbors that are *fainter* than the primary galaxies are plotted.

in the K_s filter, leading to an underestimation of the major pair fraction in the K_s filter. Most of the neighbors that do not have measurable K_s magnitude are rather faint, with the green crosses clustering toward the faint end. Although the 5 h_{100}^{-1} kpc inner cutoff guards against blending in the K_s filter at lower redshifts, in the highest redshift bin, the angular size corresponding to 5 h_{100}^{-1} kpc is small enough to allow legitimate neighbors to be identified in the z band within $\leq 1.0''$ of the host galaxy, where blending in the K_s filter can be a serious concern. On further investigation, the bias is indeed found to be more severe in case of close neighbors, with ~54% of the neighbors within $1''$ of the main galaxy not having measured K_s magnitude. Furthermore, even out of the neighbors within $1''$ of the main galaxy that have a K_s magnitude ascribed to them, ~17% are actually blended with the host galaxy. Incompleteness of the K_s-band catalog due to detection limit and blending is therefore the main reason for missing K_s magnitudes for many of the neighbors. This implies that the major merger fraction that we derive using the K_s filter is a *lower limit*. In addition, this effect is more severe at higher redshifts, leading to an underestimation of the *rate* at which the merger fraction evolves with redshift.

In the z band, on the other hand, we have verified using the z-band number counts in the GOODS-S field, that the photometric catalog is complete down to the faintest magnitude expected of a neighbor for the faintest primary galaxy ($M_J = -19.5$), even at the highest redshift (~1.2).

6. VISIBLE VERSUS NEAR-IR IDENTIFICATION OF PAIRS

As reported by Bundy et al. (2004) the selection of pairs in the visible bands may be affected by star formation; i.e., some low-mass companions may be brightened in the visible, leading to an overestimate of the actual fraction of major pairs. In order to check this assertion, we compare the $z - K_s$ color of the primary galaxy to that of the neighbors that were identified in § 5. This is shown in Figure 8 (*left*). Not surprisingly, in the K_s filter we preferentially select neighbors that are redder than the primary galaxy, while a selection in the z filter selects bluer neighbors. In the cases in which the $z - K_s$ color of the neighbor is roughly similar to that of the primary galaxy, they are picked out as major neighbors in both the filters. It must be noted, however, that neighbors are equally distributed on both sides of the $(z - K_s)_{\rm host} = (z - K_s)_{\rm neighbor}$ line. In particular, we do not find evidence for the claim made by Bundy et al. (2004) that satellite galaxies tend to be bluer than the primary galaxies. In our work the secondary galaxies can be brighter than the primary galaxies, whereas the Bundy et al. (2004) companions were always fainter than the main galaxies. In order to avoid any incompatibility in comparing our results with those of Bundy et al., we replotted Figure 8 (*right*) using only those neighbors that are fainter than the host galaxy. We again find that the neighbors are equally distributed on both sides of the $(z - K_s)_{\rm host} = (z - K_s)_{\rm neighbor}$ line. This shows intrinsically that the neighbor can be both redder as well as bluer compared to the host galaxy.

7. THE PAIR STATISTICS AND THE MERGER RATE EVOLUTION WITH REDSHIFT

Table 1 lists the primary galaxy/neighbor statistics from our work, segregated in three redshift bins for each of the two filters, z and K_s. We have defined the major merger fraction (i.e., the fraction of galaxies likely to merge) as

$$f(z) = \frac{N_{\rm pairs} + N_{\rm pairs}({\rm conf.}) - N_{\rm proj.}}{N_{\rm host}} \times 0.5 \qquad (3)$$

where $N_{\rm host}$ is the number of primary galaxies in each redshift bin, $N_{\rm pairs}$ is the number of galaxies existing in major pairs within *projected* 5 h_{100}^{-1} kpc $\leq r \leq$ 20 h_{100}^{-1} kpc of the primary galaxies in either of the two filters, $N_{\rm pairs}$(conf.) is the number of galaxies spectroscopically confirmed to be existing in major pairs, and $N_{\rm proj.}$ is the number of major neighbors expected to be found within 5 h_{100}^{-1} kpc $\leq r \leq$ 20 h_{100}^{-1} kpc of the primary galaxies by pure chance coincidence, estimated statistically using number counts of sources in either of the two filters. The factor 0.5 is the fraction of close pairs that are likely to merge as estimated by Patton et al. (1997) for $z = 0$ galaxies. This factor is possibly a function of redshift (Lavery et al. 2004), but the form of this dependence is not well established and is one of the more uncertain factors in our study. While we have corrected our pair fraction for the foreground/background contamination, we do not have at our

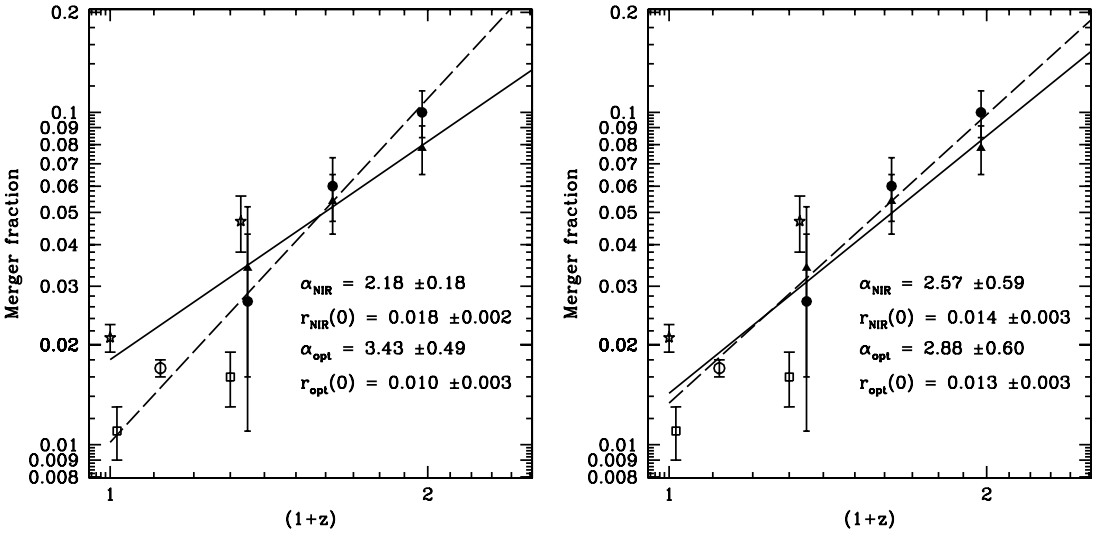

FIG. 9.—Merger fraction evolution with redshift in z filter (*filled circles*) and K_s filter (*filled triangles*). The open stars are from Patton et al. (1997), the open squares are from Patton et al. (2000, 2002), and the open circle is from the Millenium Galaxy Catalogue (De Propris et al. 2005). *Left*: Dashed line is the best-fit curve of the form $f(z) = f(0) \times (1+z)^{\alpha}$ to our z-filter data points from this work, whereas the solid line is the best-fit curve to our K_s-filter data points from this work. The lower redshift points from the literature are only shown in this panel for comparison. *Right*: Lower redshift points from literature are included in obtaining the fit so that the dashed line is the best-fit curve to our z-filter data points from this work plus all five lower redshift points from literature, and the solid line is the best-fit curve to our K_s-filter data points plus five lower redshift points.

disposal measurements of relative velocity for the two galaxies found in close pairs in most cases. For some of the pairs where we do have spectroscopic redshifts for both the members, we have put a cutoff on delta velocity $\Delta v \leq 1800$ km s^{-1} for identifying true pairs. As explained in § 5.2, this $\Delta v \leq 1800$ km s^{-1} is to be treated as an upper limit owing to the error bars on the spectroscopic redshifts used and the true delta velocity is liable to be much smaller. This justifies our use of the factor 0.5 in equation (3) following Patton et al. (2002), who have studied $z < 0.55$ galaxies in pairs with dynamical measurements and find that roughly half of those with $\Delta v < 500$ km s^{-1} are likely to be merging systems.

The evolution in the merger fraction $f(z)$ is plotted in Figure 9. In the left panel, the dashed line is the best-fit curve of the form $f(z) = f(0) \times (1+z)^{\alpha}$ to our z filter data points (*filled circles*) from this work, whereas the solid line is the best-fit curve to our K_s filter data points (*filled triangles*). The lower redshift points taken from the literature use sample selection criteria that are inconsistent with our work and are shown only for comparison. The open stars are from Patton et al. (1997), the open squares are from Patton et al. (2000, 2002), and the open circle is from the Millenium Galaxy Catalogue (De Propris et al. 2005). All of these works, with the exception of Patton et al. (1997), choose their primary sample in the rest frame B, $-21 \leq M_B \leq -18$. The difference in the slopes obtained from the two filters z and K_s can be traced back to the photometric incompleteness and blending issues in the K_s filter, as explained in detail in § 5.3.

The merger fraction shows strong evolution with redshift in both the z as well as the K_s bands. However, our derived evolution for the merger fraction suffers acutely from a lack of consistent data points at redshift ~0.0. The GOODS data set is based on a relatively small solid angle area (as expected for a deep survey) and is not ideal for deriving the merger fraction at redshifts lower than ~0.2, given the small sample size in this redshift range. On the other hand, the lower redshift estimates of merger fraction that we have available from the literature are inconsistent with our sample selection criterion and are hence not comparable. It is for this reason that we utilize the derived parameters from the fit that we have obtained using only our data set (Fig. 9*a*), even though it comes at the cost of larger error in terms of the merger rate that we finally derive.

To get an idea of how much our result is likely to change if we had a pivotal data point at redshift ~0.0, we have refitted the power-law curves, this time including the lower redshift points from literature in obtaining the fit. This is shown in Figure 9 (*right panel*), where the dashed line is the best-fit curve to our z-filter data points (*filled circles*) *plus* all five lower redshift points from literature. Similarly, the solid line is the best-fit curve to our K_s-filter data points (*filled triangle*) plus the five lower redshift points. The tacit assumption here is that the hypothetical redshift ~0.0 data point is some sort of an average of all the low-redshift data points reported in literature. We note that even in this case, the merger fraction shows strong evolution with redshift in both the z as well as the K_s bands, with the rate of evolution in the K_s filter being slightly shallower on account of the incompleteness and blending issues described earlier. Since this fit was done solely with the purpose of giving an idea to the reader of the sensitivity of our derived results to the presence/absence of a redshift ~0.0 data point, the results from this fit are not used anywhere in our work.

We used a prescription similar to that of Lin et al. (2004) to convert the merger fraction (fraction of galaxies likely to merge) into a comoving merger rate (i.e., number of merger *events* per Mpc^3 per Gyr)

$$N_{\rm mg}(z) = 0.5 n(z) f(z) \tau^{-1}, \quad (4)$$

where $n(z)$ is the comoving number density of galaxies (obtained by integrating the Pozzetti et al. [2003] luminosity function over the luminosity range of interest), $f(z)$ is the merger fraction derived above, the factor 0.5 converts the number of merging galaxies into number of merger events, and τ is the merger timescale (assumed to be 0.5 Gyr). This yielded a merger rate of 2.08×10^{-4} Mpc^{-3} Gyr^{-1} at the current epoch, which evolves by a factor of ~5.6 to 1.16×10^{-3} Mpc^{-3} Gyr^{-1} at $z = 1.2$ using K_s data.

For the z-band data, these numbers are 1.16×10^{-4} Mpc^{-3} Gyr^{-1} at the current epoch, which evolves by a factor of $\sim$15 to 1.73×10^{-3} Mpc^{-3} Gyr^{-1} at $z = 1.2$. Integrating over the timescale from $z = 1.2$ to the current epoch, we find that $41\% \pm 3.5\%$(45% $\pm$ 13% for the z filter) of galaxies with $M_J \leq -19.5$ have undergone a major merger in the last $\sim$8 Gyr. The merger timescale is generally estimated from simulations to range from 0.1 to 1 Gyr (see Hernquist and Mihos 1995), which brings an additional uncertainty to our result. For example, if it were assumed to be 0.35 Gyr (Carlberg et al. 2000), it would lead to 59% as being the fraction of galaxies having experienced a major merger in the last $\sim$8 Gyr.

7.1. *The Effect of the Large-Scale Structure in the CDFS*

As is well reported in literature (Le Fevre et al. 2004; Ravikumar et al. 2007), there are several large-scale structures in the CDFS that show up as spikes in the redshift distribution obtained from various redshift surveys. The most prominent large-scale structure is at a redshift of 0.735. It represents a factor of $\sim$10 overdensity in terms of galaxy number density. This has the potential of significantly altering the results that we have obtained for merger fraction in the redshift bin $0.5 \leq z \leq 0.75$. The detailed effect of such large-scale structures on the cosmological relevance of the GOODS south field have been considered by Ravikumar et al. (2007).

In order to check the robustness of our derived merger fraction, we recalculated the merger fraction in the redshift bin $0.5 \leq z \leq 0.75$ by excluding the sources embedded in the large-scale structure at $z = 0.735$ (defined as objects within $\delta v \leq 1500$ km s^{-1} of $z = 0.735$). This resulted in the exclusion of 70 sources from the bin $0.5 \leq z \leq 0.75$, of which 11 were major pairs (in the K_s band). The merger fraction dropped from 5.48% to 5.34%, which is well within the reported error bars. The derived merger rate is therefore not affected by the presence of the large-scale structure.

8. DISCUSSION

We have derived the major merger rates of galaxies in the redshift range $0.2 \leq z \leq 1.2$ using pair counting in both optical and near-IR bands. This work provides a robust estimate of the major merger rate up to redshift $\sim$1.2 using a representative sample of near-IR selected galaxies, which are well within the photometric completeness of the source catalogs. We find steep evolution with redshift, with the merger fraction $\propto(1+z)^{3.43\pm0.49}$ for optically selected pairs, and $\propto(1+z)^{2.18\pm0.18}$ for pairs selected in the near-IR. The difference in the slopes obtained from the two filters z and K_s can be traced back to the photometric incompleteness and blending issues in the K_s filter. We find that the major merger rate evolves by a factor of $\sim$5.6 from 2.08×10^{-4} Mpc^{-3} Gyr^{-1} at the current epoch to1.16×10^{-3} Mpc^{-3} Gyr^{-1} at $z = 1.2$. This implies that between 41% and 59% of all galaxies with $M_J \leq -19.5$ have undergone a major merger in the last $\sim$8 Gyr, assuming that the average timescale for a pair to merge is in the range 0.5–0.35 Gyr.

Our result is in agreement with the recently published results by the COSMOS team (Kartaltepe et al. 2007), who report a power-law index of 3.1 ± 0.1, as well as other works such as Le Fevre et al. (2000), Carlberg et al. (1994), and Patton et al. (2002; see Table 2 in Kartaltepe et al. 2007). Reports of a significantly lower merger rate (Lin et al. 2004; Carlberg et al. 2000) might be due to the fact that the investigators have used a luminosity evolution model for sample selection. Indeed, such a correction is not significant in our work since we have selected our sample in the rest-frame near-IR.

The disagreement in our K_s-derived merger fraction evolution with that reported by Bundy et al. (2004) might be due to their relatively small statistics (our sample size is $\sim$4 times larger than theirs), and that they did not account for neighbors that are *brighter* than the primary galaxy. Our study implies that the star formation enhancement of the companion does not severely affect the calculation of the merger rate.

We note that at least some of the discrepancies between results derived in this paper and those of other workers in the field can be attributed to different definitions of major mergers. The methodology of Lotz et al. (2008) probes a merger at a different stage in the merging process (ongoing merger), whereas our definition of major merger is sensitive to pairs of galaxies in an early stage of merger (upcoming mergers) so that two distinct members are easily distinguishable. Studies with 3D spectroscopy are certainly better suited to identifying ongoing or postmerger stages. Such studies (Flores et al. 2006; Yang et al. 2008) have found a frequent presence of complex kinematics at $z = 0.6$ (26% of $M_J < -20.3$ galaxies), which if related to mergers, is 4–5 times higher than paired/ongoing mergers found in studies like this one (see also Lotz et al. 2008). Indeed, Hammer et al. (2007) noted that all studies of merger rate agree to find $5\% \pm 1\%$ for the merger fraction at $z = 0.6$. If complex kinematics are related to mergers, it may imply a long duration (1–2 Gyr) for the remnant phase during which gaseous velocity fields are severely perturbed or chaotic (using a simple ergodic argument).

In the near future we will combine 3D spectroscopy of paired galaxies to identify the different timescales of the merging process that might shape the galaxies as we observe them today.

Finally, we note that although Toomre-type (Toomre & Toomre 1972) tidal features are seen in close pairs of galaxies in the lower redshift bins, such features are conspicuously absent in candidate pairs at higher redshifts. This is likely due to the $(1+z)^{-4}$ surface brightness dimming, which quickly pushes the low surface brightness tidal features below the detection limits at higher redshifts.

We thank the Centre Franco-Indien pour la Promotion de la Recherche Avancee (CEFIPRA) for financial assistance under project number 2804-1. A. R. would like to thank CSIR for Ph.D. funding.

REFERENCES

Bell, E. F., Phelps, S., Somerville, R. S., Wolf, C., Borch, A., & Meisenheimer, K. 2006, ApJ, 652, 270
Bertin, E., & Arnouts, S. 1996, A&AS, 117, 393
Bundy, K., et al. 2004, ApJ, 601, L123
Carlberg, R. G., Pritchet, C. J., & Infante, L. 1994, ApJ, 435, 540
Carlberg, R. G., et al. 2000, ApJ, 532, L1
De Propris, R., et al. 2005, AJ, 130, 1516
Flores, H., et al. 2006, A&A, 455, 107
Giavalisco, M., et al. 2004, ApJ, 600, L93
Hammer, F., et al. 2007, ApJ, 662, 322
Hernquist, L., & Mihos, J. C. 1995, ApJ, 448, 41
Kartaltepe, J. S., et al. 2007, ApJS, 172, 320
Lavery, R. J., et al. 2004, ApJ, 612, 679
Le Fevre, O., et al. 2000, MNRAS, 311, 565
———. 2004, A&A, 428, 1043
Lin, L., et al. 2004, ApJ, 617, L9

Lotz, J. M., et al. 2008, ApJ, 672, 177
Patton, D. R., et al. 1997, ApJ, 475, 29
———. 2000, ApJ, 536, 153
———. 2002, ApJ, 565, 208
Pozzetti, L., et al. 2003, A&A, 402, 837
Ravikumar, C. D., et al. 2007, A&A, 465, 1099
Toomre, A., & Toomre, J. 1972, ApJ, 178, 623
Vanzella, E., et al. 2005, A&A, 434, 53
———. 2006, A&A, 454, 423
Yang, Y., et al. 2008, A&A, 477, 789